Biogeosciences Discuss., 10, 14953–14998, 2013
www.biogeosciences-discuss.net/10/14953/2013/
doi:10.5194/bgd-10-14953-2013

Biogeosciences Discussions
Open Access

Surface circulation and upwelling patterns around Sri Lanka

A. de Vos, C. B. Pattiaratchi, and E. M. S. Wijeratne

School of Environmental Systems Engineering & The Oceans Institute, The University of Western Australia, 35 Stirling Highway, Crawley, Western Australia 6009, Australia

Received: 15 August 2013 – Accepted: 23 August 2013 – Published: 11 September 2013

Correspondence to: A. de Vos (asha.devos@lincoln.oxon.org)

Published by Copernicus Publications on behalf of the European Geosciences Union.

Abstract

Sri Lanka occupies a unique location within the equatorial belt in the northern Indian Ocean with the Arabian Sea on its western side and the Bay of Bengal on its eastern side. The region is characterised by bi-annually reversing monsoon winds resulting from seasonal differential heating and cooling of the continental land mass and the ocean. This study explored elements of the dynamics of the surface circulation and coastal upwelling in the waters around Sri Lanka using satellite imagery and the Regional Ocean Modelling System (ROMS) configured to the study region and forced with ECMWF interim data. The model was run for 2 yr to examine the seasonal and shorter term (~ 10 days) variability. The results confirmed the presence of the reversing current system in response to the changing wind field: the eastward flowing Southwest Monsoon Current (SMC) during the Southwest (SW) monsoon transporting 11.5 Sv and the westward flowing Northeast Monsoon Current (NMC) transporting 9.5 Sv during the Northeast (NE) monsoon, respectively. A recirculation feature located to the east of Sri Lanka during the SW monsoon, the Sri Lanka Dome, is shown to result from the interaction between the SMC and the Island of Sri Lanka. Along the eastern and western coasts, during both monsoon periods, flow is southward converging along the south coast. During the SW monsoon the Island deflects the eastward flowing SMC southward whilst along the east coast the southward flow results from the Sri Lanka Dome recirculation. The major upwelling region, during both monsoon periods, is located along the south coast and is shown to be due to flow convergence and divergence associated with offshore transport of water. Higher surface chlorophyll concentrations were observed during the SW monsoon. The location of the flow convergence and hence the upwelling centre was dependent on the relative strengths of wind driven flow along the east and west coasts: during the SW (NE) monsoon the flow along the western (eastern) coast was stronger and hence the upwelling centre was shifted to the east (west). The presence of upwelling along the south coast during both

BGD
10, 14953–14998, 2013

monsoon periods may explain the blue whale (*Balaenoptera musculus*) aggregations in this region.

1 Introduction

Sri Lanka is situated within the equatorial belt in the northern Indian Ocean, with the Arabian Sea on its western side and the Bay of Bengal on its eastern side (Fig. 1). In an oceanographic sense the location of Sri Lanka is unique with its offshore waters transporting water with different properties through reversing ocean currents, driven by monsoon winds. The northern Indian Ocean is characterised by bi-annually reversing monsoon winds resulting from the seasonal differential heating and cooling of the continental land mass and the ocean. The Southwest (SW) monsoon generally operates between June and October and the Northeast (NE) monsoon operates between December through April (Tomczak and Godfrey, 2003). The transition periods are termed the First Inter-Monsoon (May) and Second Inter-Monsoon (November). During the SW monsoon, the Southwest Monsoon Current (SMC) flows from west to east transporting higher salinity water from the Arabian Sea whilst during the NE monsoon the currents reverse in direction with the Northeast Monsoon Current (NMC) transporting lower salinity water originating from the Bay of Bengal from east to west (Schott and McCreary, 2001). During the SW monsoon, increased chlorophyll concentrations ($> 5\,\mathrm{mg\,m^{-3}}$) have been recorded around Sri Lanka, particularly along the southern coast (Vinayachandran et al., 2004) which appears to be a major upwelling region. These elevated chlorophyll concentrations persist for more than four months and have been attributed to coastal upwelling, advection by the SMC and open ocean Ekman pumping (Vinayachandran et al., 2004). Although during the SW monsoon the winds are upwelling favourable in terms of Ekman dynamics, proximity to the equator ($\sim 6^{\circ}$ N) may in fact preclude the development of wind-induced coastal upwelling. Chlorophyll concentrations during the NE monsoon appear to be low but there is evidence of high productivity through documentation of feeding aggregations of blue

BGD
10, 14953–14998, 2013

whales (*Balaenoptera musculus*) along the southern coast of Sri Lanka (de Vos et al., 2013). To date, no studies have been undertaken to define the circulation patterns and associated upwelling around Sri Lanka at a fine scale. Due to the paucity of field data, previous research has focussed on the analysis of satellite imagery and coarse resolution models designed to simulate basin scale features. In this paper we use satellite imagery and a high spatial resolution numerical model (ROMS) with realistic and idealised forcing to investigate the flow patterns and upwelling mechanisms particularly off the southern coast of Sri Lanka.

The continental shelf around Sri Lanka is narrower, shallower and steeper than is average for the world (Wijeyananda, 1997). Its mean width is 20 km, and it is narrowest on the southwest coast where it is less than 10 km (Shepard, 1963; Swan, 1983; Wijeyananda, 1997). The continental slope around Sri Lanka is a concave feature that extends from 100–4000 m in depth. The continental slope on the southern and eastern coasts has an inclination of 45° which is one of the steepest recorded globally (Sahini, 1982). The abyssal plain around the island is 3000–4000 m deep (Swan, 1983).

The seasonal difference of sea surface salinity (> 2) around Sri Lanka is highly significant compared to other regions (Levitus et al., 1994). Salinity in the Bay of Bengal is generally lower (< 33 PSU), whilst salinities in the Arabian Sea are higher with maxima up to 36.5 PSU due to high evaporation and negligible freshwater input. The Bay of Bengal receives $\sim 1500\,km^3\,yr^{-1}$ of freshwater through freshwater run-off whilst the total freshwater input into the Arabian Sea is $\sim 190\,km^3\,yr^{-1}$. Including evaporation and rain, the Arabian Sea experiences a negative freshwater supply of about $1\,m\,yr^{-1}$, whereas there is a positive freshwater supply of about $0.4\,m\,yr^{-1}$ to the Bay of Bengal (Jensen, 2001).

The mean sea level pressure (SLP) in the northern Indian region is at a maximum during December-January and a minimum during June–July with a mean seasonal range of 5–10 hPa (Wijeratne, 2003). There is significant seasonal variation in sea level in the northeastern Indian Ocean with a range in the inner Bay of Bengal of ~ 0.80–0.90 m decreasing to the south (Wijeratne, 2003). The seasonal sea level vari-

BGD
10, 14953–14998, 2013

ability around Sri Lankan waters is around 0.2–0.3 m with maxima during June through the action of the SW monsoon (Wijeratne et al., 2008). The tides around the Island are mixed semidiurnal with a maximum spring tidal range of ∼ 0.70 m.

The surface circulation of the northern Indian Ocean may be described after Schott and McCreary (2001). A schematic of the circulation in the northern Indian Ocean, in the vicinity of Sri Lanka, during the SW monsoon is shown in Fig. 2b. Along India and Sri Lanka, the eastern boundary current or West Indian Coastal Current (WICC) in the Arabian Sea flows southwards along the West Indian coastline and joins the eastward flowing Southwest Monsoon Current (SMC). Shankar et al. (2002) also postulated a westerly flow from the south central Arabian Sea entraining water into the SMC. The presence of the anti-clockwise Lakshadweep eddy off the southwest coast of India modifies the current flow in this region. The SMC flows along the south coast of Sri Lanka from west to east (Schott et al., 1994) transporting ∼ 8 Sv ($1\,Sv = 106\,m^3\,s^{-1}$). After passing the coast of Sri Lanka, the currents form an anti-clockwise eddy defined as the Sri Lanka Dome (SD) centered around 83° E and 7° N (Vinayachandran and Yamagata, 1998). The western arm of this eddy drives a southward current along the eastern coast of Sri Lanka whilst the remainder flows northward along the eastern Indian coast as the East Indian Coastal Current (EICC).

During the NE monsoon the currents reverse in direction (Fig. 2a). Along the eastern Indian coast, the EICC flows southward past Sri Lanka and joins the Northeast Monsoon Current (NMC) flowing from east to west transporting about 12 Sv (Schott et al., 1994). The currents then flow around the clockwise Lakshadweep eddy and northward along the western Indian coastline as the West Indian Coastal Current (WICC).

One of main features to note from this description from the perspective of Sri Lanka, is the reversal of currents along the western and southern coasts and the north to south flow along the eastern coast. This circulation pattern is confirmed by Shankar et al. (2002). However, Varkey et al. (1996) and Shankar and Shetye (1997) both provide a different interpretation and suggest that currents along the east coast of Sri Lanka

BGD
10, 14953–14998, 2013

flow south to north irrespective of season. Hence, the circulation along the eastern coast of Sri Lanka remains to be resolved.

The upwelling off the south coast of Sri Lanka usually appears and intensifies during the summer months when the SW monsoon prevails, and is said to be due to a combination of wind driven Ekman transport, advection by the SMC and open ocean Ekman pumping (McCreary Jr. et al., 2009; Vinayachandran et al., 2004; Vinayachandran et al., 1999). Monthly satellite image composites of chlorophyll analysed by Yapa (2009) show high productivity waters with mean chlorophyll concentrations $>5\,\mathrm{mg\,m^{-3}}$ along the southern and western regions during the months of June-August that are accompanied by a 2° to 3 °C decrease in sea surface temperature (SST) corresponding to regions where high chlorophyll a concentrations are detected. To illustrate this relationship, MODIS images indicate the strong relationship between higher chlorophyll and cooler SSTs (Fig. 3). Data collected during the Dr. Fridtjof Nansen cruises between 1978 and 1989 provide evidence that the SW monsoon bloom results from upwelling that begins closer to the coast and progresses further offshore as it develops over subsequent months (Saetersdal et al., 1999). Michisaki et al. (1996) confirmed high primary productivity when they recorded maximum nitrate concentrations of approximately 10 µM in mid-June accompanied by maximum chlorophyll concentrations of $0.9\,\mathrm{mg\,m^{-3}}$ off the west coast of Sri Lanka.

The aim of this paper is to define the seasonal changes in circulation and upwelling patterns around Sri Lanka using a high resolution numerical model (ROMS) including realistic forcing complemented by satellite imagery. The motivation for the paper is the observation of blue whale (*Balaenoptera musculus*) feeding aggregations off the southern coast of Sri Lanka during the NE monsoon period (de Vos et al., 2013) despite satellite imagery indicating lower productivity in the surface waters. This paper is organised as follows; In Sect. 2, we describe the numerical model configuration and validation; Sect. 3 presents the results from analysis of the wind fields, satellite imagery and numerical model output including idealised simulations to examine upwelling gen-

BGD
10, 14953–14998, 2013

eration mechanisms and the results are discussed in Sect. 4 with overall conclusions given in Sect. 5.

2 Methodology

The main approach for the study is the use of a numerical model to identify the mean circulation patterns and upwelling around Sri Lanka. There is a lack of field data from this region and some of the available public domain data have been accessed and presented in this paper. The data include: wind speed and direction data from a coastal meteorological station located at Hambantota (Fig. 1); meteorological information from ECMWF ERA interim data which were also used for model forcing; and MODIS satellite imagery (ocean colour and SST) accessed from the ocean colour website (Feldman and McClain, 2013).

2.1 ROMS configuration and validation

The Regional Ocean Modelling System (ROMS) is a three-dimensional numerical ocean model based on the nonlinear terrain following coordinate system of Song and Haidvogel (1994). ROMS solves the incompressible, hydrostatic, primitive equations with a free sea surface, horizontal curvilinear coordinates, and a generalized terrain-following s-vertical coordinate that can be configured to enhance resolution at the sea surface or seafloor (Haidvogel et al., 2008). The model formulation and numerical algorithms are described in detail in Shchepetkin and McWilliams (2005), and have been used to simulate the circulation and upwelling processes in a range of ocean basins (e.g. Di Lorenzo et al., 2007; Dong et al., 2009; Haidvogel et al., 2008; Marchesiello et al., 2003; Xu et al., 2013).

The model grid (Fig. 1) configured for this study included the continental shelf and slope waters surrounding Sri Lanka as well as the deeper ocean and consisted of a horizontal grid with resolution < 2 km with 30 vertical layers in a terrain-following s-

BGD
10, 14953–14998, 2013

coordinate system. The minimum model depth was set to −15 m, i.e. coastal regions shallower than 15 m were set to 15 m. The model was driven by direct air-sea interface heat and freshwater fluxes, momentum fluxes, inverted barometric effects, tide/sea level, transport and tracers at open boundaries. The forcing data were interpolated onto the corresponding model grid points to create initial and forcing files. The model was driven with 3 hourly atmospheric forcing and daily surface heat and freshwater fluxes using ECMWF ERA interim data. HYCOM global ocean model (Bleck, 2002) daily outputs of salinity, temperature, and horizontal velocities were used to specify the open boundary section 3-D tracers and transport. Open boundary barotropic velocities were estimated by vertically averaging the eastward (u) and northward (v) component data, which were interpolated at the boundary sections. At open boundaries ROMS offers a wide array of conditions. We used a combination of nudging and radiation conditions for 3-D transport and tracers at the model open boundaries. The model forcing tides were derived from the TPX07.2 global tidal model and monthly climatological mean sea levels derived from the AVISO database. The tides were provided as complex amplitudes of earth-relative sea-surface elevation and tidal currents for eight primary harmonic constituents (M_2, S_2, N_2, K_2, K_1, O_1, P_1, Q_1). These harmonics were introduced in ROMS through the open boundaries elevation using the Chapman and current ellipse variable using the Flather condition (see Marchesiello et al., 2001). Model hindcast simulations were undertaken to obtain optimal model results. Three-dimensional variables (salinity, temperature and velocity components) were output at daily intervals with sea surface heights at hourly intervals.

2.2 Experimental setup

In addition to realistic simulations to examine the seasonal circulation patterns and upwelling, numerical experiments were also designed to address the following: (1) role of land-mass effect contribution to upwelling around Sri Lanka; (2) variability in the upwelling centre in response to the magnitude and direction of winds along the western and eastern sides of the Island; and, (3) mechanisms for the formation of the Sri Lanka

BGD
10, 14953–14998, 2013

Dome located to the east of Sri Lanka. In order to address (1), model simulations were undertaken including and excluding the Coriolis term whilst model runs with synthetic wind fields were undertaken to examine (2), with different wind stress on the western and eastern sides of Sri Lanka. Mechanisms for the formation of the Sri Lanka Dome (3) were explored by forcing the model with constant westerly winds of different magnitudes (2, 4, 6 and 8 ms^{-1}). Additional model runs (not presented here) were also undertaken to investigate whether the tides played a role in the upwelling process.

2.3 Model validation

Model hindcasts were undertaken over a 2 yr period (2010 and 2011) using realistic surface and boundary forcing (Sect. 2.1). The first year (2010) was considered as spin up and results presented here are from the second year (2011) of simulations. In the absence of detailed field measurements from the region, predicted surface currents and temperature distributions were compared with available data as well as with sea level data.

2.3.1 Tide and mean sea level

The predicted hourly sea levels at each grid point were subjected to harmonic analysis using the T-Tide MATLAB toolbox (Pawlowicz et al., 2002). To visualise and interpret model results obtained around Sri Lanka, co-tidal charts for the main tidal constituents, M_2, S_2, K_1, and O_1, were produced (not shown). The predicted amplitudes and phases from the simulation are in close agreement with measured data for four major tidal constituents (Table 1). The spring tidal range, $2(M_2 + S_2)$ varies from nearly zero to 0.60 m along the coastline, the minimum range occurred at the southeast and northwest corners and the maximum range occurred at the central part of the western and northeastern corners. The tidal phases on the east coast of Sri Lanka feature opposite phases from the west coast for the M_2 and S_2 constituents with a rapid phase change at the southeast and northwest corners. These features of the tidal characteristics are

BGD
10, 14953–14998, 2013

in agreement with Wijeratne (2003). The diurnal (K_1 and O_1) tidal amplitudes are small (< 0.1 m) around the Island.

2.3.2 Large-scale circulation

Shipboard ADCP current measurements for the region are available from the World Ocean Circulation Experiments (WOCE). However, it is important to note that there were no observations during the model simulation period (2010 and 2011). We compared the model results and observations based on time of year as shown in Fig. 4. It is clear that there is good qualitative agreement between the predicted and observed currents throughout the ship tracks. The model results also reproduce some of the observed circulation features. For example, seasonal reversal of currents along the south coast during the two monsoon periods is reproduced: during the NE monsoon the currents flow towards the west (Fig. 4a and b) whilst during the SW monsoon they flow to the east (Fig. 4c and d). The reversing current pattern to the east of Sri Lanka during the NE monsoon with southward currents close to the coast and northward currents further offshore is also reproduced (Fig. 4a). The model also reproduced fine-scale features that were represented in the ADCP transect such as the transition from west to eastward currents closer to the coast (Fig. 4c).

2.3.3 Satellite imagery

Suspended material (such as sediment, chlorophyll etc) in the surface waters may be used as a passive tracer to follow flow patterns using satellite imagery (Pattiaratchi et al., 1987). In regions of upwelling (for example see Fig. 3), there is also a correspondence between regions of higher surface chlorophyll concentrations (SCC) and lower sea surface temperatures (SST). Thus, ocean colour imagery may be used to qualitatively validate numerical model outputs. Comparison between model predicted SST and satellite derived SCC indicate that the model reproduced observed patterns, particularly the higher chlorophyll 'tongue' feature, and sharp fronts (Fig. 5).

BGD
10, 14953–14998, 2013

3 Results

3.1 The wind field

The monsoon and inter-monsoon periods occur at similar times during the year. However, there is an interannual variability in the onset of these climatic events and thus the timing of each monsoon can vary by up to 1–2 months. Wind data recorded in 2010, from a coastal meteorology station located along the southeast coast of Sri Lanka (Hambantota, Fig. 1), reflects changes in the wind field in accordance with the monsoons (Fig. 6): winds blew from between the north and east (0–90°) from December to April whilst the winds were predominantly from the southwest and west (225—270°) between April to November (Fig. 6). Wind speeds were $\sim 8\,ms^{-1}$ between mid-January and mid-March corresponding to the peak of the NE monsoon; $< 6\,ms^{-1}$ between mid-March and mid-May (waning NE monsoon and first inter-monsoon); increased to $> 6\,ms^{-1}$ from June until October reflecting the SW monsoon and decreased to $< 6\,ms^{-1}$ during the second inter-monsoon period in mid-November.

In addition to the temporal changes in the wind field there is also significant spatial distribution as revealed by the ECMWF ERA interim data (Fig. 7). One of the factors influencing the spatial wind field is the local land topography of Sri Lanka and southern India. Coastal regions around Sri Lanka are relatively flat and surround the elevated central region that increases to a maximum elevation of 2500 m. Similarly, southern India consists of elevated terrain that exceeds 1,000 m (Luis and Kawamura, 2000). During the NE monsoon (Fig. 7a and f), winds are predominantly from the northeast across the study region with stronger winds in the Gulf Mannar (Fig. 1) as a result of local land topography. Here, the northeasterly winds are funneled through the elevated topography between southern India and Sri Lanka resulting in strong winds over the Gulf of Mannar (Luis and Kawamura, 2000). Off the southern coast of Sri Lanka, the winds are weaker and are mainly offshore during the NE monsoon (Fig. 7a and f). During the first inter-monsoon, the east coast of Sri Lanka experiences onshore winds (easterly) with northeasterly winds along the west coast and winds off the south coast

BGD
10, 14953–14998, 2013

remaining offshore (Fig. 7b). Along the western and southern coasts of Sri Lanka, during the SW monsoon, the winds are westerly (Fig. 7c, d and e) and, due perhaps to the local topography, they veer northwards off the eastern side of the island (south-westerly winds). As such, both the temporal and spatial wind field influences the ocean circulation patterns around the island.

3.2 Seasonal circulation

3.2.1 Satellite imagery

The seasonal circulation around Sri Lanka was examined through the use of surface chlorophyll concentration (SCC) climatology data (resolution of 4 km from Feldman and McClain, 2013) as a passive tracer and to understand seasonal variability in surface chlorophyll concentrations.

In January, the Northeast Monsoon Current (NMC) flows from east to west (Fig. 8a). This is reflected in the SCC data with slightly higher concentrations to the west of Sri Lanka. However, the more pronounced feature is the "stirring" caused by the NMC flowing from east to west past the Maldives island chain with enhanced SCC to the west of the island chain. During this period, the monsoon drift is shallow and will generally only have a minimal effect on the waters below the thermocline (Wyrtiki, 1973). In March, during the monsoon transition period, SCC decreased to $< 0.20\,\mathrm{mgm}^{-3}$ (Fig. 8b) in the whole study region. There is an absence of a 'concentration wake' in the vicinity of the Maldive islands indicating weak currents lacking unidirectionality in this region. Similar conditions were observed in April (not shown). In May, during the onset of the SW monsoon (Fig. 7c), a band of high SCC ($\sim 2.5\ \mathrm{mgm}^{-3}$) water was present along the south coast of Sri Lanka (Fig. 8c) and also in the Gulf of Mannar. SCC levels along the south coast were 10 times higher than they were in April but low concentrations were present to the east of Sri Lanka. In June (not shown), the high SCC patch off southern India begins to extend to the east across the entrance to the Gulf of Mannar, whilst surrounding areas experienced decreased SCC. In July, enhanced SCC to the east of the

BGD
10, 14953–14998, 2013

Maldive islands and the plume of elevated SCC to the southeast of Sri Lanka confirmed the eastward flow of the Southwest Monsoon Current (Fig. 8d). The high SCC plume generated by the SW monsoon current flowing past the Maldive islands, merged with the high SCC patch off southern India and the higher SCC waters off the west coast of Sri Lanka (Fig. 8d). The SCC is now ∼5 mgm^{-3} along the west and southern coasts of Sri Lanka. A plume of higher SCC water originating from the southern coast of Sri Lanka extended to the east and shows evidence of an eddy – most likely the Sri Lanka Dome (Fig. 2b). There is also a band of lower SCC water adjacent to the east coast of Sri Lanka, which is due to the southward flow of water along this coast at this time of year. In September, the SCC patterns were similar to that in July (Fig. 8e) except the maximum SCC was lower in the range of 0.20–0.40 mgm^{-3} and extended over a larger area particularly to the south and east of Sri Lanka. In November, the SCC levels decreased almost to those observed in January, the difference being the plume from the Maldive Islands was present to the east indicating that the SMC was still flowing eastwards (Fig. 8f).

In general, chlorophyll a concentrations around Sri Lanka were relatively lower during the NE monsoon compared to the SW monsoon (Kabanova, 1968). This seasonality is maintained year to year but with interannual variability (Fig. 9). A Hovmöller diagram of monthly mean SSC between the southern coast of Sri Lanka (6° N) and the equator indicates higher values closest to the Sri Lankan coast extending ∼2700 km offshore on average. In 2002 and 2006, the influence of this upwelling can be observed extending to the equator. Although interannual variability is not within the scope of this paper it is interesting that 2002 and 2006 reflect El Nino and positive Indian Ocean dipole years (Sreenivas et al., 2012).

3.2.2 Numerical modelling

Numerical model results reproduce the general patterns identified in previous studies (Fig. 2) and from ocean colour imagery (Fig. 8). The seasonal mean currents show significant spatial variability due to the spatial and temporal changes in the wind climate

BGD
10, 14953–14998, 2013

(Fig. 10). This is evident when comparing the mean currents during the NE monsoon (Fig. 10a) and the instantaneous currents at the end of December (Fig. 4a and b). The reversing currents to the south of Sri Lanka: easterly during the SW monsoon and westerly during the NE monsoon are reproduced by the model. The currents during the SW monsoon are stronger than those during the other seasons reflecting the stronger winds during this period (Fig. 10c). Schott and McCreary (2001) estimated that off southern Sri Lanka (north of the equator) transport rates resulting from the SMC and NMC were 8 and 12 Sv respectively, with SMC transport rates lower than those for the NMC. The numerical model output indicates transport rates of 11.5 and 9.5 Sv for the SMC and NMC respectively. These values are more realistic in that the NMC transport is similar to that estimated by Schott and McCreary (2001) but SMC transport is higher, as expected due to the stronger winds experienced during this period.

During the NE monsoon, currents along the east coast of Sri Lanka flow southwards closer to the coast and northwards further offshore, separated by a shear zone (Figs. 10a, 4a and b). The presence of the shear zone is confirmed by a shipborne ADCP transect (Fig. 4a). The currents closer to the shore follow the coastline, flowing to the west along the south coast and northward along the west coast (Figs. 10a, 4a and b). Currents in the Gulf of Mannar flow towards the southwest and mirror the direction of the wind (Fig. 10a). During the first inter-monsoon, current speeds decrease (Fig. 10b) with currents along both the east and west coasts converging off southern Sri Lanka (south of $\sim 6.5^{\circ}$ N). The presence of the Sri Lanka Dome centred at 84° E and 8° N can be identified. Strong northward currents along the northeast coast extending along the southern Indian coastline are predicted. This flow pattern is similar to that shown on satellite images by Legeckis (1987) postulating a western boundary current in the Bay of Bengal.

Under SW monsoon conditions, currents are higher across the entire region, particularly along the south and southeast coasts of Sri Lanka (Fig. 10c). As a result, the Sri Lanka Dome shifts to the north – now centered at 84° E, 9.5° N. Southward flowing water along the east coast converges with water eastward of the SMC. There is also

BGD
10, 14953–14998, 2013

a stronger band of currents flowing past the southern tip of India and the west of Sri Lanka (Fig. 10c) which explains the merging of the SCC between the southern regions of the Indian coast and Sri Lanka (Fig. 8d). The weakest currents are predicted during the second inter-monsoon with no evidence of the Sri Lanka Dome (Fig. 10d).

Flow patterns such as those described in Fig. 10 provide no indication on regions and periods of coastal upwelling around Sri Lanka. Therefore, the model predicted sea surface temperature (SST) and flow fields were examined at shorter time-scales with the assumption that cooler waters (compared to the surrounding water) represented upwelling. Analysis of model output revealed that upwelling occurs on a seasonal basis and/or during shorter period sporadic events along different parts of the coastline. During the NE monsoon, cooler SSTs were observed along the western and southern coasts with warmer water along the east coast of Sri Lanka (Fig. 11a). The latter is due to the downwelling regime in this region with onshore winds during the NE monsoon reflected in a band of narrow warm southward moving water. Colder waters were found in regions of divergence in the flow field where there was mainly offshore transport of water (Fig. 11a) reflecting that perhaps processes other than wind-driven upwelling may be responsible for the upwelling. There was negligible colder surface water present during the first inter-monsoon period except perhaps along the extreme north of Sri Lanka (Fig. 11b). The southern coastal regions of both India and Sri Lanka experienced colder SST throughout the SW monsoon indicating strong upwelling during this period (Fig. 11c and d). There was also advection of colder water from the southern tip of India to the west coast of Sri Lanka during the SW monsoon (Fig. 11c and d). The most notable feature is the shape of the cold water regions to the south and southeast of Sri Lanka (Fig. 11c and d, respectively). This shape is clearly visible on satellite images as a result of the associated higher SCC (Figs. 2 and 5) and occurs in regions of convergence: in July 2011 (Figs. 3, 11c) water flowing southwards along both the east and west coasts converges to the south and is transported offshore resulting in a colder water patch near the coast. In August, this colder water patch migrates to the east and is present off the southeast coast of Sri Lanka (Fig. 11d). This feature is very

BGD
10, 14953–14998, 2013

similar to that observed in the August 2012 satellite image (Fig. 3c and d). These features indicate that wind driven upwelling through Ekman dynamics is most likely not responsible for upwelling along the south coast of Sri Lanka.

3.3 Temporal (10 day) variability

In order to assess the shorter period spatial variability of surface circulation and upwelling around Sri Lanka, model output for surface currents and temperature averaged over a 10 day period, were examined. Initially, during the NE monsoon (January 2011) southward currents flowed along both the east and west coasts of Sri Lanka with easterly currents along the south coast (Fig. 12a). The currents appear to converge along the southeast corner as indicated by the presence of colder water. Over the next 10 days, the currents along the eastern coast increased due to stronger winds and this is accompanied by a reversal in the currents along the south coast, which flow eastwards causing the convergence zone (and colder water due to upwelling) to shift towards the southeast (Fig. 12b). During the subsequent 10 day period, there is colder water along the entire west coast of Sri Lanka including the Gulf of Mannar due to upwelling and a contribution through cooling due to air-sea fluxes (e.g. (Luis and Kawamura, 2000). Analysis of scatterometer (NSCAT) winds by Luis and Kawamura (2000) indicated a 15-day periodicity in the wind field and these changes in the circulation patterns may reflect the temporal changes associated with the wind field. Shorter period spatial variability during January and July are shown in Figs. 9 and 10, respectively. ROMS simulations suggest that a small change in the direction of the currents incident on the Island can change the nature of the current patterns around the island and the location of the upwelling centre. This will be further analysed in the next section.

During the SW monsoon the eastward flowing SMC dominates the region. However, there is a similarity in the current fields to those observed during the NE monsoon: currents along both the western and eastern coasts flow southwards with a region of convergence either along the south or southeast coast of Sri Lanka (Fig. 13). Here over a 40-day period the convergence zone progressively migrates from the south coast to

BGD
10, 14953–14998, 2013

the east coast. As a result, the cold water region associated with the convergence of the currents also migrates to the east. The SST patterns predicted by the model are very similar to those observed in the satellite imagery (cf. Figs. 13 and 3c and d).

The model results and satellite imagery for both the NE and SW monsoon periods indicate that in general southward currents flow along both coasts of Sri Lanka resulting in a convergence region along the southern half of the island. During the NE monsoon, this convergence region migrates to the west (Fig. 12) whilst during the SW monsoon the convergence region migrates to the east (Fig. 13). Idealised model runs were undertaken to investigate the mechanisms causing this migration which was hypothesised to be due to different wind stresses on each of the coasts. Three idealised model runs were undertaken with constant northerly winds as follows (1) wind stress of 0.28 Pa off the east coast and 0.14 Pa along the west coast; (2) wind stress of 0.28 Pa along both coasts; and, (3) wind stress of 0.14 Pa off the east coast and 0.28 Pa along the west coast (i.e. the opposite of (1)). The results indicated that when the wind stress was equal along both coasts the upwelling region was located directly off the south coast (Fig. 14) whilst when the wind stress was stronger on the west (east) coast the upwelling region migrated to the east (west). Thus the location of the upwelling appears to be controlled by the relative strengths of the winds along each coast, which changes with season due to the changing monsoon. However, the surface currents and upwelling were much stronger during the SW monsoon compared to that during the NE monsoon due to the increased wind strengths.

3.4 Sri Lanka Dome

One of the major features observed during the SW monsoon period is the presence of the Sri Lanka Dome (SD, Fig. 2). Here, the SMC flows eastward along the south coast of Sri Lanka and creates a recirculation in the lee (east) of Sri Lanka with the western arm creating a southward current along the east coast. The features of the dome were identified in the satellite climatology (Fig. 8d) and in the numerical model output (Fig. 10c). Analysis of the climatological thermal structure along 85°E by Vinay-

BGD
10, 14953–14998, 2013

achandran and Yamagata (1998) indicated well-developed upward doming isotherms and they attributed the presence of the dome to open ocean Ekman pumping. The SD is analogous to flow patterns in the lee of headlands and islands with the Island of Sri Lanka acting as a headland interacting with the eastward flowing SMC (e.g. Pattiaratchi et al., 1987). A series of idealised model runs were undertaken to examine the hypothesis that the SD is formed through the interaction between the SMC and topography. Here, 15 day model runs with constant westerly winds of 2, 4, 6 and 8 ms^{-1} were undertaken. The wind speeds selected were based on observed winds (Fig. 6) and westerly winds were prescribed in the model as this was the main direction of winds to the west of Sri Lanka during the SW monsoon (Fig. 7). The results indicate that for all four cases, a recirculation occurred in the lee of Sri Lanka. The recirculation strengthened (increased in vorticity) with an increase in the wind speed although the location of the centre remained at the same location around 84° E and 7–8° N with a slight migration to the east with increasing wind stress. These results indicate that the primary formation mechanism of the SD is the interaction between the SMC and the landmass of Sri Lanka. This does not rule out the possibility that Ekman pumping may play a role in strengthening the dome.

4 Discussion

The seasonal and shorter term (~10 days) changes in the surface circulation and upwelling patterns around Sri Lanka were examined using satellite imagery (mainly ocean colour) and a high spatial resolution numerical model (ROMS) configured to the study region and forced with ECMWF interim data. The model reproduced all of the documented major circulation features in the region: reversing monsoon currents in response to the changing wind field and the Sri Lanka Dome. The model predictions of sea surface temperature patterns were similar to those observed by satellite imagery. Model output was used to update the transport rates of the SMC and NMC between Sri Lanka and the equator. Using a current meter array located to the south of Sri Lanka

BGD
10, 14953–14998, 2013

Schott et al. (1994) estimated transport rates of 8 and 12 Sv for SMC and NMC. These values are contradictory in that with stronger SW monsoon winds it would be expected that SMC transport rates are higher than those for the NMC. The numerical model output indicates transport rates of 11.5 and 9.5 Sv for SMC and NMC respectively, which are likely more realistic. The values for the NMC are similar to those estimated by Schott et al. (1994) but that for the SMC is now higher. It should be noted that the estimates by Schott et al. (1994) were through the analysis of moored current meters, which did not sample the top 30 m of the water column.

Sri Lanka is a relatively large island (length 440 km; width 225 km) and, as mentioned in the Introduction, is situated in a unique geographic location in terms of oceanographic processes: experiencing seasonally reversing monsoon currents that interact with the Island. Many studies have reported the influence of flow interaction with islands and headlands leading to enhanced primary production – termed the island mass effect (IME) by Doty and Oguri (1956). These studies have included different spatial scales using laboratory and field experiments to understand circulation and enhanced productivity. They include those in the vicinity of oceanic islands: Johnston atolls (Barkley, 1972), Aldabra and Cosmoledo atolls (Heywood et al., 1990), Barbados (Bowman et al., 1996; Cowen and Castro, 1994), Canary Islands (Barton et al., 2000), the Kerguelen Islands (Bucciarelli et al., 2001), Madeira Island (Caldeira et al., 2002), Galapagos (Palacios, 2002), Hawaii Islands (Hafner and Xie, 2003), Santa Catalina (Dong and McWilliams, 2007); and, in continental shelf and coastal regions: Wolanski et al. (1984), Pattiaratchi et al. (1987) and Alaee et al. (2007). Many scaling arguments have been proposed to define the circulation patterns in the lee of islands based on the Reynolds number which appear to reproduce the circulation in the lee of the island/headland (Tomczak, 1988; Wolanski et al., 1984). The predicted flow patterns around Sri Lanka are indicative of flow patterns observed in other regions both in deep and shallow water; however, due to the reversing flow patterns there are two distinct patterns that can be identified:

BGD
10, 14953–14998, 2013

1. During the SW monsoon, the SMC interacts with the Island which acts more as a headland as there is minimal flow through Palk Strait, the channel between India and Sri Lanka (Fig. 1). The flow follows the curvature of the southern coast of Sri Lanka and generates a lee eddy in the form of the Sri Lanka Dome. Using values of L$\sim$200 km; $U \sim 0.8\,\mathrm{ms}^{-1}$; and $K_h \sim 10^4\,\mathrm{m}^2\,\mathrm{s}^{-1}$, yields a Reynolds number ($R_e = UL/K_h$; U – velocity scale, L – length scale and K_h – horizontal eddy viscosity; Tomczak, 1988) of $\sim$20 which predicts an attached eddy which is the Sri Lanka Dome (Fig. 1). This is confirmed by the idealised model runs with constant westerly winds which predict a stronger eddy with increasing wind (flow) speeds (Fig. 15).

2. During both the SW and NE monsoons, the model results indicated southward flow along both east and west coasts converging along the south coast. In this case, circulation is similar to that of an Island with no discernible wake – defined as attached flow (e.g. Alaee et al., 2004). The currents are now weaker and using values of $L \sim 100$ km; $U \sim 0.1$ ms^{-1}; and $K_h \sim 10^4\,\mathrm{m}^2\,\mathrm{s}^{-1}$, yields a Reynolds number $R_e = \sim 1$, in line with the theoretical predictions.

Flow along the south coast of Sri Lanka in both monsoons is subject to curvature which can lead to secondary circulation (Alaee et al., 2004). Here, as a result of the curvature induced centrifugal acceleration the surface waters move offshore and are replaced by water from the sub-surface. In the case of Sri Lanka, although located close to the equator, scaling reveals that the Coriolis force is important in the dynamics (Rossby Number $R_o < 1$) and that according to the flow regime proposed by Alaee et al. (2004) flow curvature is negligible in the generation of the secondary circulation when compared to the Coriolis force (Regime B where $R_o < 1$ and $R_e > 1$). To further investigate the importance of the Coriolis term, model simulations were undertaken with the inclusion and exclusion of the Coriolis force during the SW monsoon. The results indicate that when the Coriolis force was omitted there was no upwelling (colder water) to the west of Sri Lanka, particularly off the south Indian coast (Fig. 16). The

BGD
10, 14953–14998, 2013

upwelling feature with convergent flow to the southeast of the island is present in both simulations but is enhanced and pronounced in the model run with the inclusion of the Coriolis force. Hence, although the Coriolis force is important in the dynamics of the region, it does not appear to play a major role in the upwelling along the south coast of Sri Lanka.

In terms of upwelling patterns, case (1) clearly indicates the presence of higher SCC within the Sri Lanka Dome (Fig. 8) and Vinayachandran and Yamagata (1998) indicated well-developed upward doming isotherms in a climatological cross section of the dome. The main upwelling observed in the satellite imagery, both in terms of climatology (Fig. 3) and individual dates (Fig. 8) indicate the dominant upwelling regions along the south coast of Sri Lanka. Examining the climatological monthly means indicates a wide band of higher SCC offshore of the southern coast which could be attributed to wind driven coastal upwelling due to Ekman dynamics. However, individual satellite images and numerical model outputs indicate that the mechanism of upwelling is more complicated. Located in the tropics the region is frequently under cloud cover and cloud free satellite imagery is very limited. Examination of the complete 10 yr archived daily images in the ocean colour imagery database (Feldman and McClain, 2013) yielded less than 10 cloud free images for the region. However, these images often indicate similar patterns of upwelling where there is a 'tongue' (triangular shape) of high SCC water with the wider section attached to the coast and tapering offshore (Fig. 3). The location of this tongue varied along the south coast and was present during both SW and NE monsoon periods. Similar high SCC patterns were reported by Vinayachandran et al. (2004) (Fig. 3). Although the numerical model did not include a biophysical model to simulate phytoplankton growth (chlorophyll) the predicted SST distribution was remarkably similar to the higher SCC patterns and the associated SST patterns observed by satellite (Fig. 3). The model output indicated that the lower SST patterns were associated with regions of convergence: currents from both east and west coasts converged in the upwelling centre defined by lower SST and the idealised model runs indicated that the location of the upwelling centre was dependent on the relative wind stress

BGD
10, 14953–14998, 2013

along each coast. During the NE monsoon the upwelling centre was shifted to the west whilst during the SW monsoon the upwelling centre was shifted to the east (Fig. 14). It should also be noted that the south coast of Sri Lanka has a narrow continental shelf hence shelf processes as a primary mechanism for upwelling may be neglected. There are no previous studies which have addressed this type of circulation pattern and upwelling: interaction between convergent flows around an island leading to upwelling. The island of Taiwan has a similar oceanographic setting with northward currents along both coastlines converging to the north of the island with upwelling along the northeast corner (Chang et al., 2010). However, numerical experiments indicate that there is re-circulation to the north of the Island and the upwelling is due mainly to the Kuroshio Current encroaching onto the shelf (Chang et al., 2010). On a smaller scale, Magnell et al. (1990) show enhanced upwelling at Cape Mendocino resulting from converging currents at the tip of the Cape. Through continuity, horizontal divergence at the sea surface results in vertical upwelling of water from depth. The numerical model results, confirmed by the high SCC patterns, confirm this process: the currents flowing parallel to the eastern and western coasts converge along the south coast and are deflected offshore. As the water flows offshore, there is divergence of water at the coast which results in upwelling of colder water from depth. This was confirmed by the numerical model output which indicated a lower sea surface height at the centre of upwelling.

The observation of blue whales (*Balaenoptera musculus*) feeding off the southern coast of Sri Lanka during the NE monsoon period (de Vos et al., 2013) provided the motivation for this study. The NE winds, under Ekman dynamics, would generate a downwelling system (onshore Ekman flow), along the south coast of Sri Lanka resulting in a low primary productive system. The results of this study are able to explain that the upwelling system along the south coast of Sri Lanka is not driven by Ekman dynamics rather through an interaction of the wind driven circulation around the Island. This results in a converging coastal current system that flows offshore creating a divergence at the coastline resulting in upwelling which is able to maintain a relatively higher productivity system during both monsoon periods.

BGD
10, 14953–14998, 2013

5 Conclusions

This paper has explored the elements of the dynamics of the surface circulation and coastal upwelling in the waters around Sri Lanka, located in the northern Indian Ocean, a region influenced by seasonally reversing monsoon winds through satellite imagery and a numerical model. Numerical model predictions compared well with the limited field data and satellite observations. The main conclusions may be summarised as follows:

1. The results confirmed the presence of the eastward flowing Southwest Monsoon Current (SMC) during the SW monsoon and the westward flowing Northeast Monsoon Current (NMC), respectively. The predicted transport for the SMC and NMC of 11.5 and 9.5 Sv respectively are more realistic than previous estimates.

2. Sri Lanka Dome, a recirculation feature located to the east of Sri Lanka during the SW monsoon is the result of the interaction between SMC and the Island resulting in a recirculation eddy. It is possible that the eddy is enhanced through wind stress curl.

3. During both monsoon periods, the flow off the east and west coasts are southward, converging along the south coast. During the SW monsoon the Island deflected the eastward flowing SMC southward whilst along the east coast the southward flow results from the Sri Lanka Dome recirculation.

4. The major upwelling region, during both monsoon periods, is located along the south coast and results from flow convergence and associated offshore transport of water. Higher SCC values were observed during the SW monsoon. The location of the flow convergence and hence the upwelling centre was dependent on the relative strengths of wind driven flow along the east and west coasts: during the SW (NE) monsoon the flow along the western (eastern) coast was stronger and hence the upwelling centre was shifted to the east (west).

BGD
10, 14953–14998, 2013

Acknowledgements. A. de Vos is supported by a UWA Scholarship for International Research Fees (SIRF).

References

Alaee, J. M., Ivey, G., and Pattiaratchi, C.: Secondary circulation induced by flow curvature and Coriolis effects around headlands and islands, Ocean Dynam., 54, 27–38, 2004.

Alaee, J. M., Pattiaratchi, C. B., and Ivey, G. N.: Numerical simulation of the summer wake of Rottenest Island, Western Australia, Dynam. Atmos. Oceans, 43, 171–198, 2007.

Barkley, R. A.: Johnston Atoll's wake, J. Mar. Res., 30, 210–216, 1972.

Barton, E. D., Basterretxea, G., Flament, P., Mitchelson-Jacob, E. G., Jones, B., Arístegui, J., and Herrera, F.: Lee region of Gran Canaria, J. Geophys. Res., 105, 173–117, 2000.

Hybrid Coordinate Ocean Model (HYCOM) http://www.hycom.org, 2002.

Bowman, M. J., Dietrich, D. E., and Lin, C. A.: Observations and modelling of mesoscale ocean circulation near a small island, in: Small Islands: Marine Science and Sustainable Development, Coastal and Estuarine Studies, edited by: Maul, G., American Geophysical Union, Washington DC, 18–35, 1996.

Bucciarelli, E., Blain, S., and Tréguer, P.: Iron and manganese in the wake of the Kerguelen Islands (Southern Ocean), Mar. Chem., 73, 21–36, 2001.

Caldeira, R. M. A., Groom, S., Miller, P., Pilgrim, D., and Nezlin, N. P.: Sea-surface signatures of the island mass effect phenomena around Madeira Island, Northeast Atlantic, Remote Sens. Environ., 80, 336–360, 2002.

Chang, Y.-L., Oey, L.-Y., Wu, C.-R., and Lu, H.-F.: Why are there upwellings on the northern shelf of Taiwan under northeasterly winds?, J. Phys. Oceanogr., 40, 1405–1417, doi:10.1175/2010jpo4348.1, 2010.

Cowen, R. K. and Castro, L. R.: Relation of coral reef fish larval distributions to island scale circulation around Barbados, West Indies, Bull. Mar. Sci., 54, 228–244, 1994.

de Vos, A., Kaltenberg, A. M., Friedlaender, A., Cripps, E., Harcourt, R., Pattiaratchi, C., and Nowacek, D. P.: Spatial distribution of blue whales off southern Sri Lanka in relation to prey and oceanographic parameters, Mar. Ecol.-Prog. Ser., in review, 2013.

Di Lorenzo, E., Moore, A. M., Arango, H. G., Cornuelle, B. D., Miller, A. J., Powell, B., Chua, B. S., and Bennett, A. F.: Weak and strong constraint data assimilation in the inverse Regional

BGD
10, 14953–14998, 2013

Ocean Modeling System (ROMS): Development and application for a baroclinic coastal upwelling system, Ocean Model. Online, 16, 160–187, 2007.
Dong, C. and McWilliams, J. C.: A numberical study of island wakes in the Southern California Bight, Cont. Shelf. Res., 27, 1233–1248, 2007.
Dong, C., Idica, E. Y., and McWilliams, J. C.: Circulation and multiple-scale variability in the Southern California Bight, Prog. Oceanogr., 82, 168–190, 2009.
Doty, M. S. and Oguri, M.: The island mass effect, J. Conservation, 22, 33–37, 1956.
Ocean Color Web: ocean color homepage http://oceancolor.gsfc.nasa.gov/, last access: 10 June, 2013.
Hafner, J. and Xie, S.-P.: Far-field simulation of the Hawaiian wake: Sea surface temperature and orographic effects, J. Atmos. Sci., 60, 3021–3032, doi:10.1175/1520-0469(2003)060<3021:fsothw>2.0.co;2, 2003.
Haidvogel, D. B., Arango, H., Budgell, W. P., Cornuelle, B. D., Curchitser, E., Di Lorenzo, E., Fennel, K., Geyer, W. R., Hermann, A. J., Lanerolle, L., Levin, J., McWilliams, J. C., Miller, A. J., Moore, A. M., Powell, T. M., Shchepetkin, A. F., Sherwood, C. R., Signell, R. P., Warner, J. C., and Wilkin, J.: Ocean forecasting in terrain-following coordinates: Formulation and skill assessment of the Regional Ocean Modeling System, J. Comput. Phys., 227, 3595–3624, 2008.
Heywood, K. J., Barton, E. D., and Simpson, J. H.: The effects of flow disturbance by an oceanic island, J. Mar. Res., 48, 55–73, 1990.
Jensen, T. G.: Arabian Sea and Bay of Bengal exchange of salt and tracers in an ocean model, Geophys. Res. Lett., 28, 3967–3970, doi:10.1029/2001gl013422, 2001.
Kabanova, J. G.: Primary production of the northern part of the Indian Ocean, Oceanology, 8, 214-225, 1968.
Legeckis, R.: Satellite observations of a western boundary current in the Bay of Bengal, J. Geophys. Res.-Oceans., 92, 12974–12978, doi:10.1029/JC092iC12p12974, 1987.
Levitus, S., Burgett, R., and Boyer, T. P.: World ocean atlas 1994, NOAA Atlas NESDIS 3, US Government Printing Office, Washington, DC, 1994.
Luis, A. J. and Kawamura, H.: Wintertime wind forcing and sea surface cooling near the south India tip observed using NSCAT and AVHRR, Remote Sens. Environ., 73, 55–64, 2000.
Magnell, B. A., Bray, M. A., Winant, C. D., Greengrove, C. L., Largier, J. L., Borchardt, F., Bernstein, R. L., and Dorman, C. E.: Convergent shelf flow at Cape Mendocino, Oceanography, 3, 4-11, 1990.

BGD
10, 14953–14998, 2013

Marchesiello, P., McWilliams, J. C., and Shchepetkin, A.: Open boundary conditions for long-term integration of regional oceanic models, Ocean Model. Online, 3, 1–20, 2001.
Marchesiello, P., McWilliams, J. C., and Shchepetkin, A.: Equilibrium structure and dynamics of the California current system, J. Phys. Oceanogr., 33, 753–783, 2003.
McCreary Jr., J. P., Murtugudde, R., Vialard, J., Vinayachandran, P. N., Wiggert, J. D., Hood, R. R., Shankar, D., and Shetye, S.: Biophysical processes in the Indian Ocean, Geophys. Monogr. Ser., 185, 9–32, doi:10.1029/2008GM000768, 2009.
Michisaki, R. P., Chavez, F. P., Friederich, G. E., and Kelley, M.: Evolution of chemical and biological properties in the Arabian Sea and Indian Ocean during 1995 from automated surface mapping, American Geophysical Union Ocean Sciences meeting, San Diego, 1996,
Palacios, D. M.: Factors influencing the island-mass effect of the Galápagos Archipelago, Geophys. Res. Lett., 29, 2134, doi:10.1029/2002gl016232, 2002.
Pattiaratchi, C., James, A., and Collins, M.: Island wakes and headland eddies: A comparison between remotely sensed data and laboratory experiments, J. Geophys. Res.-Oceans., 92, 783–794, doi:10.1029/JC092iC01p00783, 1987.
Pawlowicz, R., Beardsley, B., and Lentz, S.: Classical tidal harmonic analysis including error estimates in MATLAB using T_TIDE, Computers Geosci., 28, 929–937, 2002.
Saetersdal, G., Bianchi, G., Stomme, T., and Venema, S. C.: The Dr. Fridtjof Nansen Programme 1975–1993: Investigations of fishery resources in developing countries, History of the programme and review of results, Food and Agriculture Organisation of the United Nations, Rome, 434 pp., 1999.
Sahini, A.: The structure, sedimentation and evolution of Indian continental margins, in: The ocean basins and margins: The Indian Ocean, edited by: Nairn, E. M. and Stehli, F. G., Plenum Press, New York, 353–398, 1982.
Schott, F. A. and McCreary, J., J.P.: The monsoon circulation of the Indian Ocean, Prog. Oceanogr., 51, 1–123, 2001.
Schott, F., Reppin, J., Fischer, J., and Quadfasel, D.: Currents and transports of the monsoon current south of Sri Lanka, J. Geophys. Res.-Oceans, 99, 25127–25141, 1994.
Shankar, D. and Shetye, S. R.: On the dynamics of the Lakshadweep high and low in the southeastern Arabian Sea, J. Geophys. Res.-Oceans, 102, 12551–12562, 1997.
Shankar, D., Vinayachandran, P. N., and Unnikrishnan, A. S.: The monsoon currents in the north Indian Ocean, Prog. Oceanogr., 52, 63–120, 2002.

BGD
10, 14953–14998, 2013

Shchepetkin, A. F. and McWilliams, J. C.: The regional oceanic modeling system (ROMS): A split-explicit, free-surface, topography-following-coordinate oceanic model, Ocean Model. Online, 9, 347–404, 2005.
Shepard, E. P.: Submarine geology, Harper and Row Publishers, New York, 1963.
Song, Y. and Haidvogel, D.: A semi-implicit ocean circulation model using a generalized topography-following coordinate system, J. Comput. Phys., 115, 228–244, 1994.
Sreenivas, P., Gnanaseelan, C., and Prasad, K. V. S. R.: Influence of El Niño and Indian Ocean Dipole on sea level variability in the Bay of Bengal, Glob. Planet. Change, 80/81, 215–225, 2012.
Swan, B.: An Introduction to the Coastal Geomorphology of Sri Lanka, National Museums of Sri Lanka, Colombo, 1983.
Tomczak, M.: Island wakes in deep and shallow water, J. Geophys. Res., 93, 5153–5154, 1988.
Tomczak, M. and Godfrey, J. S.: Regional oceanography: An introduction, 2 ed., Pergamon, 2003.
Varkey, M. J., Murty, V. S. N., and Suryanarayana, A.: Physical oceanography of the Bay of Bengal and Andaman Sea, in: Oceanogr. Mar. Biol. Annu. Rev., edited by: Ansell, A. D., Gibson, R. N., and Barnes, M., CRC Press, 1–70, 1996.
Vinayachandran, P. N. and Yamagata, T.: Monsoon response of the sea around Sri Lanka: Generation of thermal domes and anticyclonic vortices, J. Phys. Oceanogr., 28, 1946–1960, doi:10.1175/1520-0485(1998)028<1946:mrotsa>2.0.co;2, 1998.
Vinayachandran, P. N., Masumoto, Y., Mikawa, T., and Yamagata, T.: Intrusion of the south-west monsoon current into the Bay of Bengal, J. Geophys. Res.-Oceans, 104, 11077–11085, doi:10.1029/1999JC900035, 1999.
Vinayachandran, P. N., Chauhan, P., Mohan, M., and Nayak, S.: Biological response of the sea around Sri Lanka to summer monsoon, Geophys. Res. Lett., 31, doi:10.1029/2003GL018533, 2004.
Wijeratne, E. M. S.: Tidal characteristics and modelling of tidal wave propagation in shallow lagoons of Sri Lanka, Ph.D., Gothenburg University, Gothenburg, 2003.
Wijeratne, E. M. S., Woodworth, P. L., and Stepanov, V. N.: The seasonal cycle of sea level in Sri Lanka and southern India, West Indian Ocean J. Mar. Sci., 7, 29–43, 2008.
Wijeyananda, N. P.: Maritime zones, in: Arjuna's atlas of Sri Lanka, edited by: Somasekaram, T., Perera, M., de Silva, M. B. G., and Godellawatta, H., Arjuna Consulting Company Limited, Colombo, 5–7, 1997.

BGD
10, 14953–14998, 2013

Wolanski, E., Imberger, J., and Heron, M. L.: Island wakes in shallow coastal waters, J. Geophys. Res., 89, 553–569, 1984.

Wyrtiki, K.: Physical oceanography of the Indian Ocean, in: The Biology of the Indian Ocean, edited by: Zeitzschel, B. and Gerlach, S. A., Springer-Verlag, Heidelberg, 1973.

Xu, J., Lowe, R. J., Ivey, G. N., Pattiaratchi, C. B., Jones, N. L., and Brinkman, R.: Dynamics of the summer shelf circulation and transient upwelling off Ningaloo Reef, Western Australia, J. Geophys. Res.-Oceans, 118, 1099–1125, 2013.

Yapa, K. K. A. S.: Upwelling phenomena in the southern coastal waters of Sri Lanka during southwest monsoon period as seen from MODIS, Sri Lanka J. Phys., 10, 7–15, 2009.

BGD
10, 14953–14998, 2013

Table 1. Tidal constituents at different stations along the coastline of Sri Lanka. Tide gauge data are denoted in regular font and model data are denoted in italic font. Phase refers to local time.

Station	M_2				S_2				K_1				O_1			
	a (m)		g^o		a (m)		g^o		a (m)		g^o		a (m)		g^o	
Trincomalee	0.18	*0.19*	238	*252*	0.06	*0.08*	268	*276*	0.07	*0.06*	332	*338*	0.02	*0.01*	304	*343*
Batticaloa	0.14	*0.14*	235	*227*	0.07	*0.06*	265	*279*	0.05	*0.04*	330	*310*	0.02	*0.02*	300	*267*
Oluwil	0.07	*0.05*	230	*248*	0.03	*0.02*	260	*245*	0.05	*0.06*	332	*324*	0.01	*0.01*	280	*253*
Kirinda	0.07	*0.06*	92	*88*	0.056	*0.06*	130	*112*	0.031	*0.03*	29	*358*	0.01	*0.01*	17	*10*
Galle	0.16	*0.17*	56	*48*	0.11	*0.09*	99	*112*	0.05	*0.06*	21	*69*	0.01	*0.03*	73	*112*
Colombo	0.18	*0.18*	45	*48*	0.12	*0.12*	93	*115*	0.07	*0.06*	32	*48*	0.03	*0.03*	58	*76*
Chilaw	0.18	*0.19*	045	*0.57*	0.11	*0.12*	092	*114*	0.09	*0.08*	43	*55*	0.03	*0.04*	058	*86*
Delft Island	0.11	*0.11*	38	*42*	0.04	*0.035*	77	*84*	0.11	*0.08*	76	*57*	0.05	*0.06*	006	*24*
Kayts	0.03	*0.02*	63	*78*	0.01	*0.008*	96	*126*	0.12	*0.09*	61	*145*	0.02	*0.03*	77	*123*
Point Pedro	0.16	*0.18*	242	*256*	0.09	*0.08*	270	*245*	0.05	*0.06*	328	*277*	0.01	*0.03*	003	*347*

BGD
10, 14953–14998, 2013

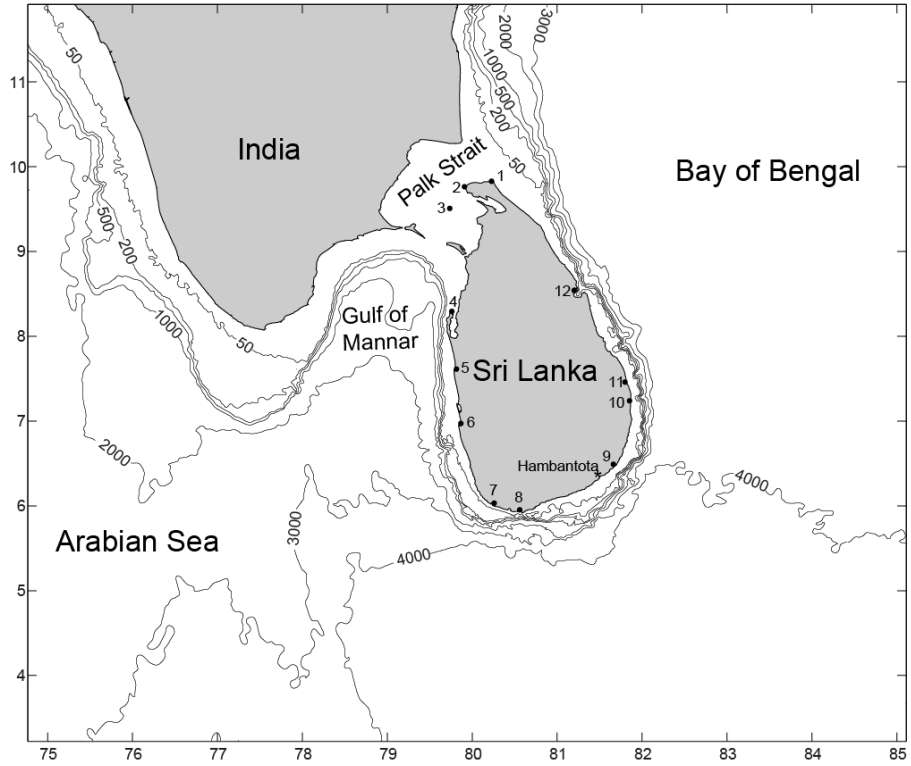

Fig. 1. Study area showing bathymetry and model domain. Numbers represent tide stations used for model validation. 1. Point Pedro 2. Kayts 3. Delft Island 4. Kalpitiya 5. Chilaw 6. Colombo 7. Galle 8. Dondra 9. Kirinda 10. Oluwil 11. Batticaloa 12. Trincomalee. Wind speed and direction data was from the Hambantota Meteorological Station on the southeast coast.

BGD
10, 14953–14998, 2013

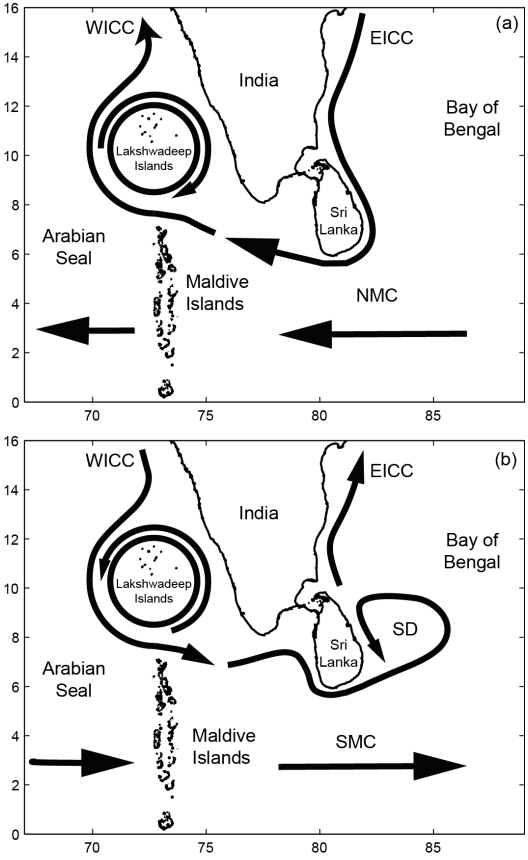

Fig. 2. Circulation patterns around Sri Lanka and southern India for **(a)** Northeast monsoon and **(b)** Southwest monsoon. Where WICC is West Indian Coastal Current; EICC is East Indian Coastal Current; SMC is Southwest Monsoon Current; NMC is Northeast Monsoon Current and SD is Sri Lanka Dome.

BGD
10, 14953–14998, 2013

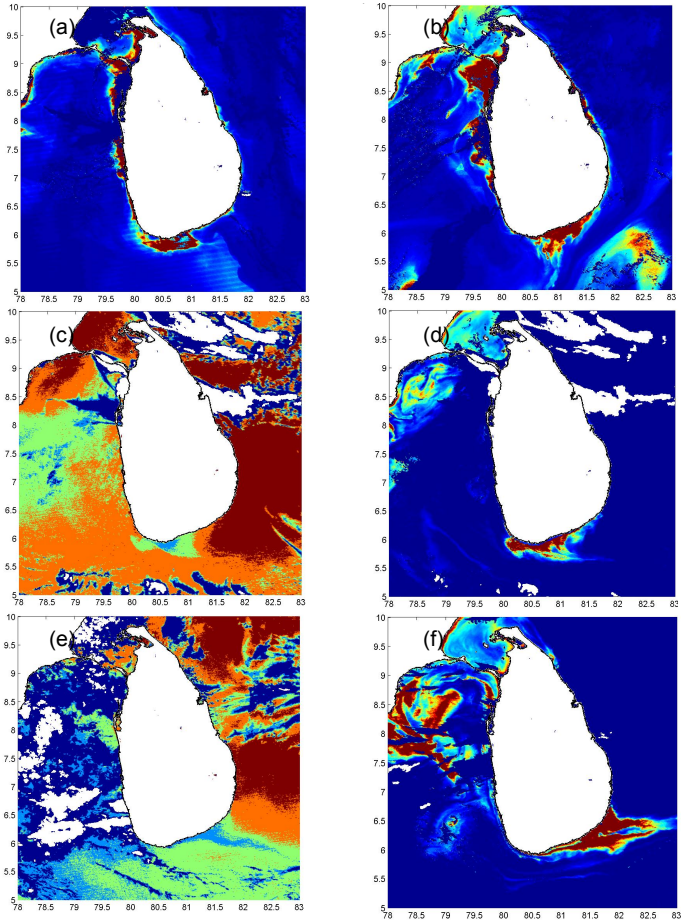

Fig. 3. Caption on next page.

BGD
10, 14953–14998, 2013

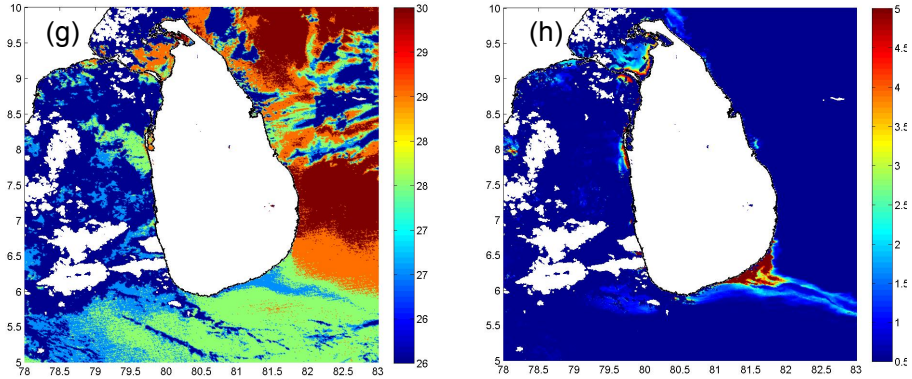

Fig. 3. (a) Surface Chlorophyll concentration (SCC) obtained on 13 December 2010; **(b)** SCC on 21 January 2011; **(c)** Sea Surface Temperature (SST) on 19 October 2003; **(d)** SCC on 19 October 2003; **(e)** SST on 1 August 2012; **(f)** SCC on SST on 1 August 2012; **(g)** SST on 19 June 2013; **(h)** SCC on 19 June 2013. The chlorophyll and temperature scales are on **(g)** and **(h)** respectively and apply to all images.

BGD
10, 14953–14998, 2013

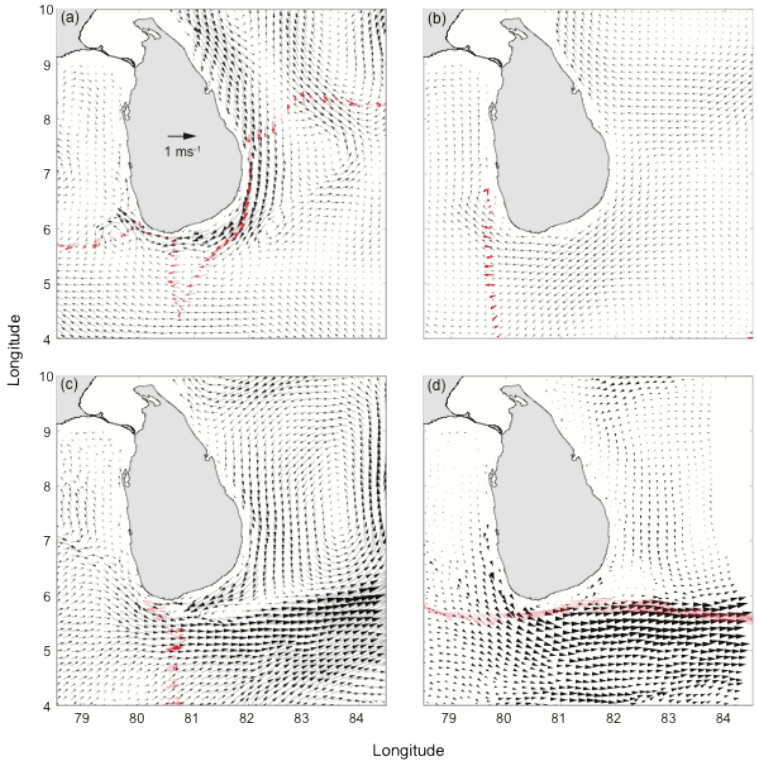

Fig. 4. Comparison of the shipboard ADCP measured (red) and ROMS (blue) currents at 30 m depth. **(a)** ADCP from 25–31 December 1997 and ROMS for 31 December 2010, **(b)** ADCP from 01 to 05 March 1995 and ROMS for 3 March 2011, **(c)** ADCP from 21–30 July 1993 and ROMS for 26 July 2011 and **(d)** ADCP from 1–3 August 2005 and ROMS for 3 August 2011.

BGD
10, 14953–14998, 2013

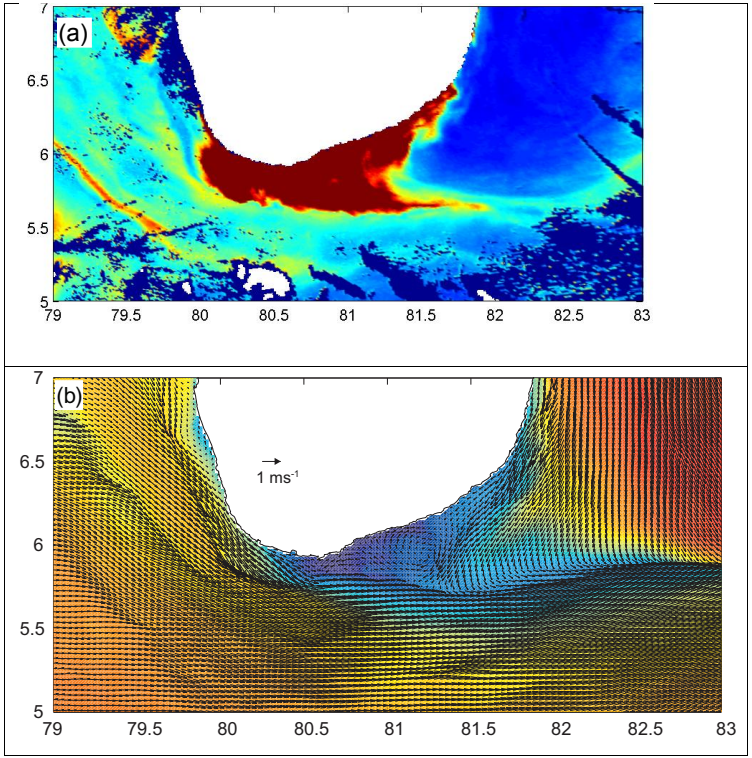

Fig. 5. Typical summer upwelling frontal features around southern part of Sri Lanka obtained on 12 October 2003 **(a)** satellite derived surface chlorophyll concentration; **(b)** Predicted near-surface current vectors and temperature.

BGD
10, 14953–14998, 2013

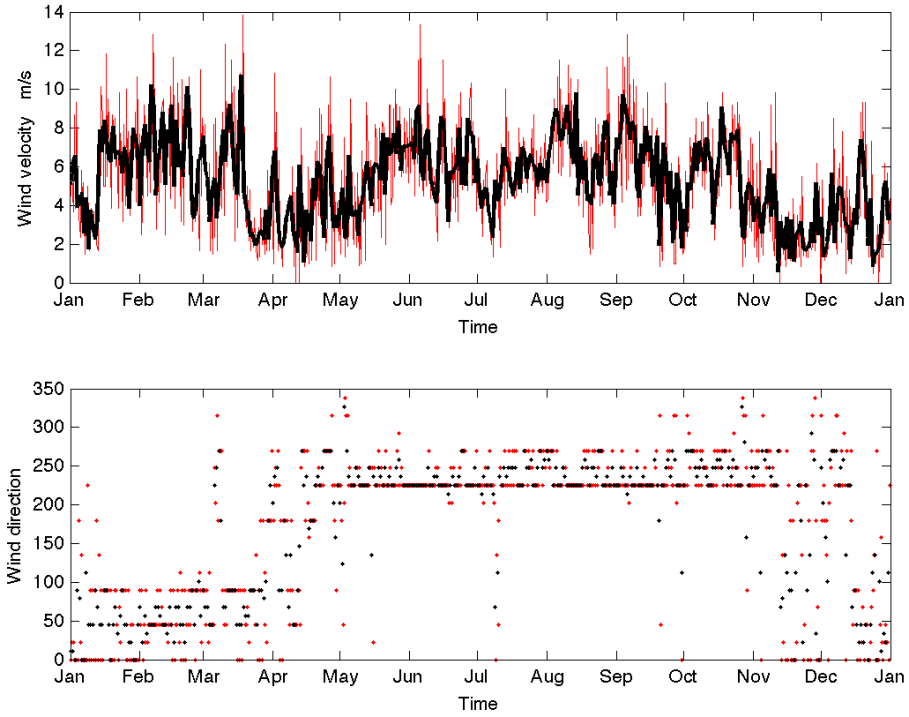

Fig. 6. Time series for wind speed and direction for Sri Lanka in 2010. The red line and dots indicate daily data collected at 0830 hrs and 1730 h and black line and dots indicate the daily averaged data. Data were obtained from the Hambantota meteorological station, southeast Sri Lanka.

BGD
10, 14953–14998, 2013

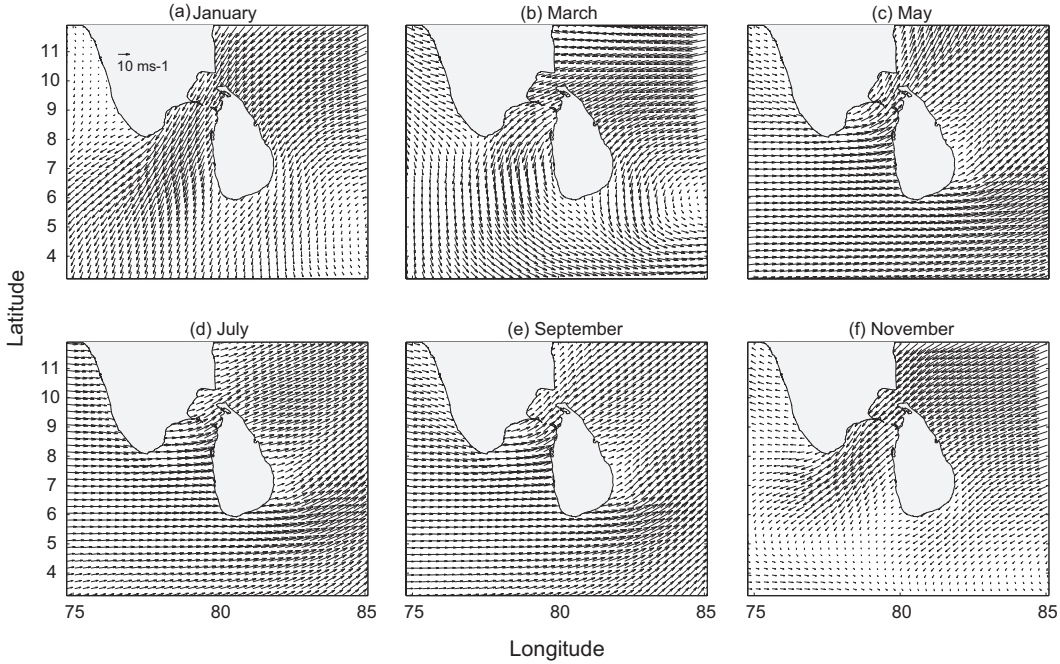

Fig. 7. Bi-monthly wind speed and direction for Sri Lanka in 2011 from ECMWF ERA interim data. Each plot represents a bi-monthly average with length of arrow correlating with speed. **(a)** January (northeast monsoon); **(b)** March (first inter-monsoon); **(c)** May, **(d)** July and **(e)** September (southwest monsoon); **(f)** November (second inter-monsoon).

BGD
10, 14953–14998, 2013

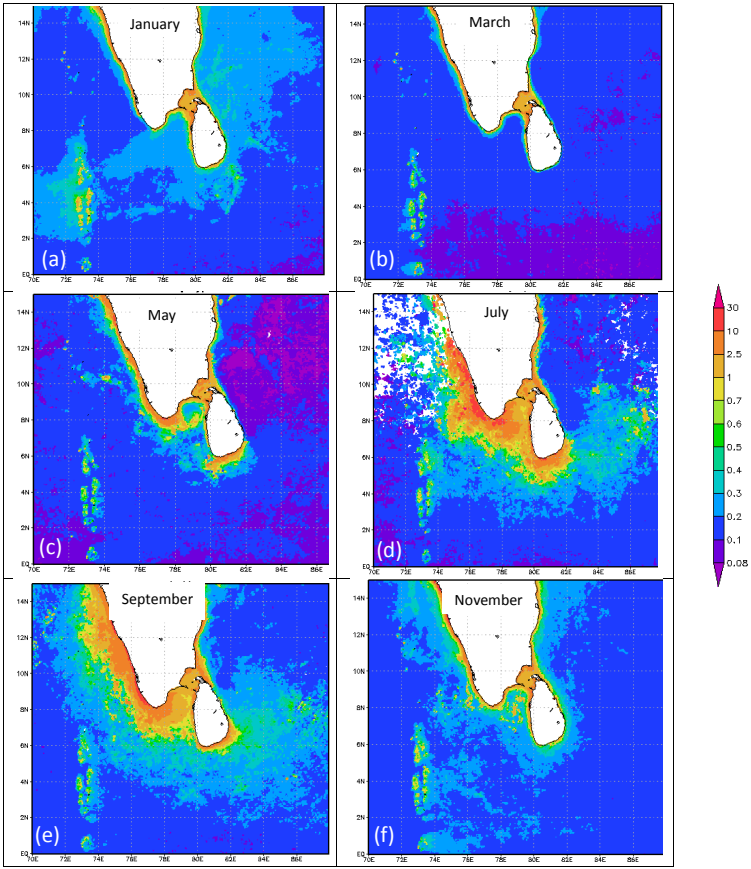

Fig. 8. Monthly mean surface chlorophyll concentrations around Sri Lanka, obtained from climatology. **(a)** January; **(b)** April; **(c)** May; **(d)** July; **(e)** September; **(f)** November.

BGD
10, 14953–14998, 2013

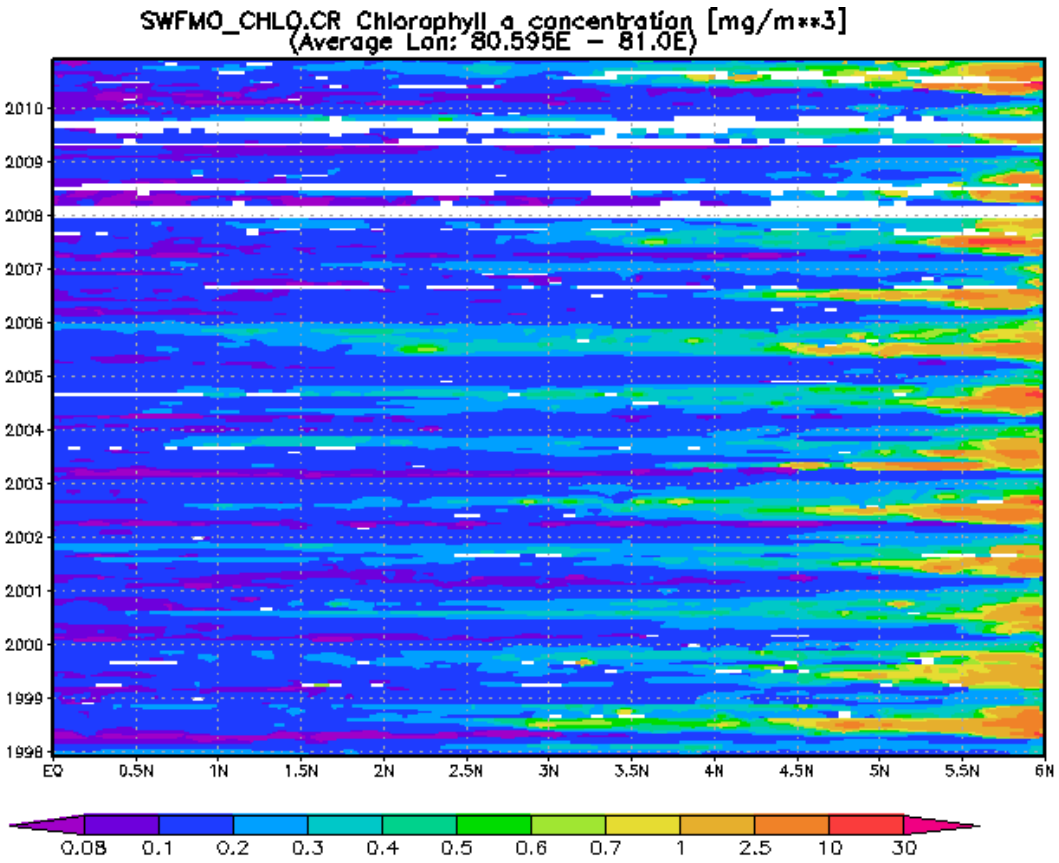

Fig. 9. *Hovmöller* diagram displaying seasonality and inter-annual variability of surface chlorophyll concentrations off the southern coast of Sri Lanka.

BGD
10, 14953–14998, 2013

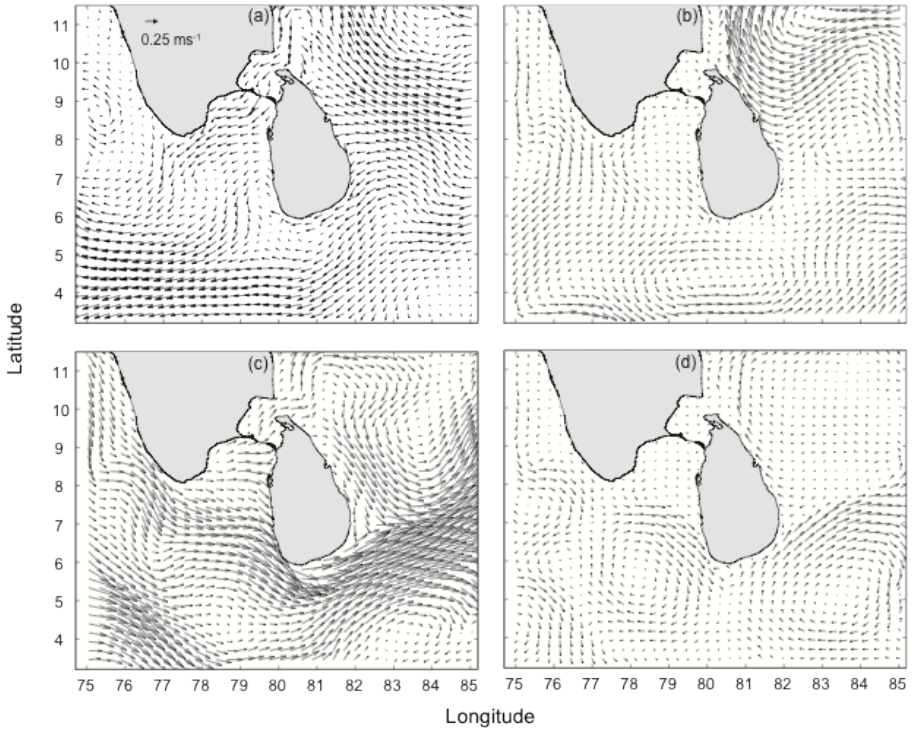

Fig. 10. Seasonal circulation from ROMS **(a)** January; **(b)** April; **(c)** July; **(d)** October.

BGD
10, 14953–14998, 2013

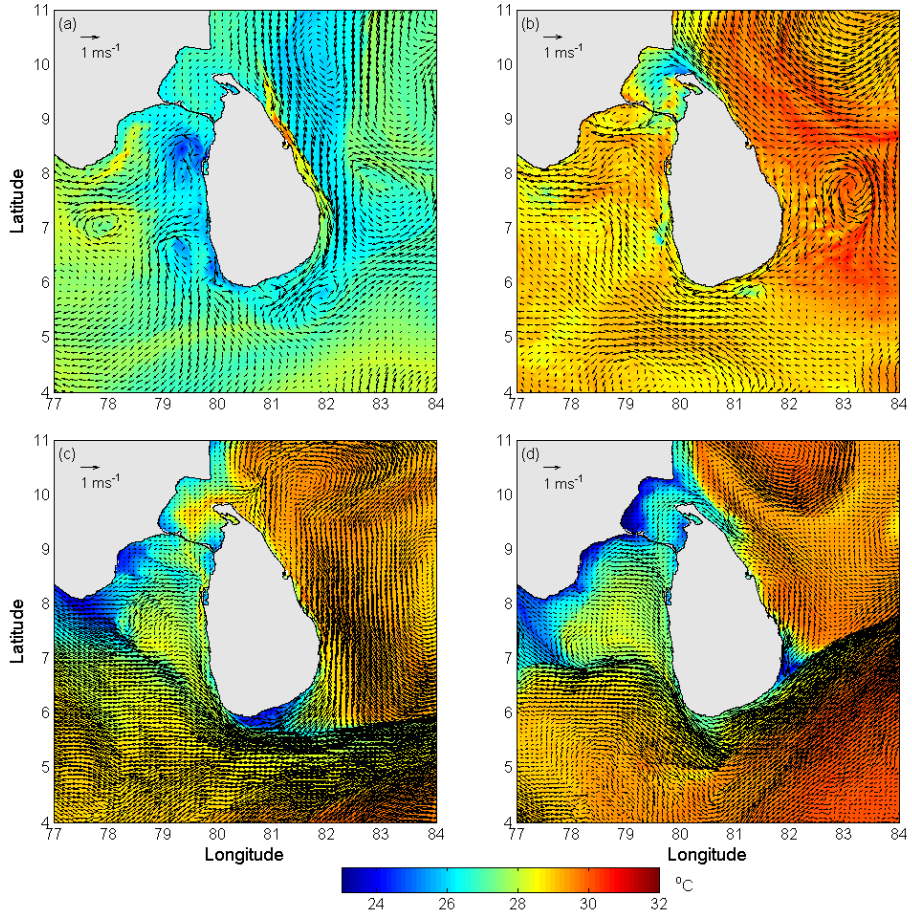

Fig. 11. Predicted near-surface current vectors plotted on the surface temperature showing major upwelling regions around Sri Lanka **(a)** 16–20 January 2011; **(b)** 10–14 April 2011; **(c)** 12–16 July 2011 and **(d)** 18–22 August 2011.

BGD
10, 14953–14998, 2013

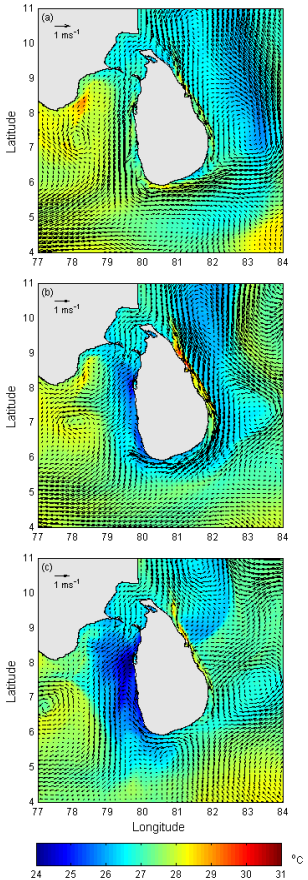

Fig. 12. Predicted near-surface current vectors plotted on the surface temperature showing sporadic upwelling **(a)** 1–10 January 2011 **(b)** 11–20 January 2011 and **(c)** 21–31 January 2011.

BGD
10, 14953–14998, 2013

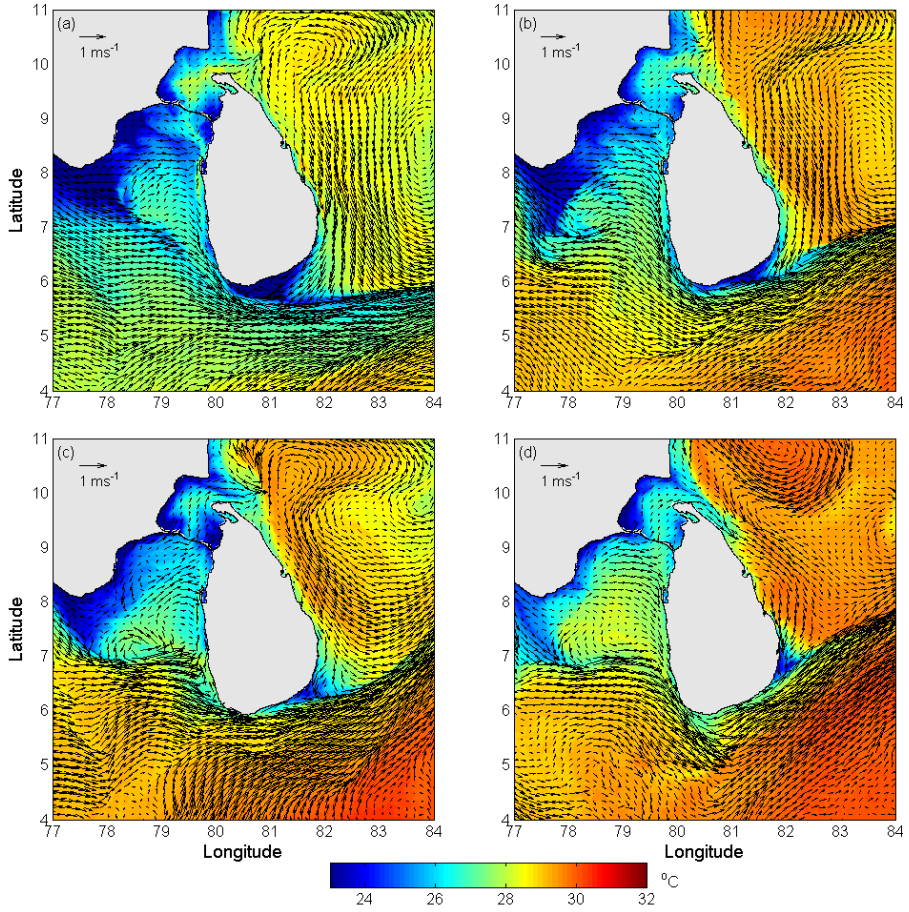

Fig. 13. Model-computed near-surface current vectors plotted on the surface temperature showing upwelling centre shift **(a)** 12 July 2011 **(b)** 22 July 2011, **(c)** 2 August 2011, **(d)** 12 August 2011.

BGD
10, 14953–14998, 2013

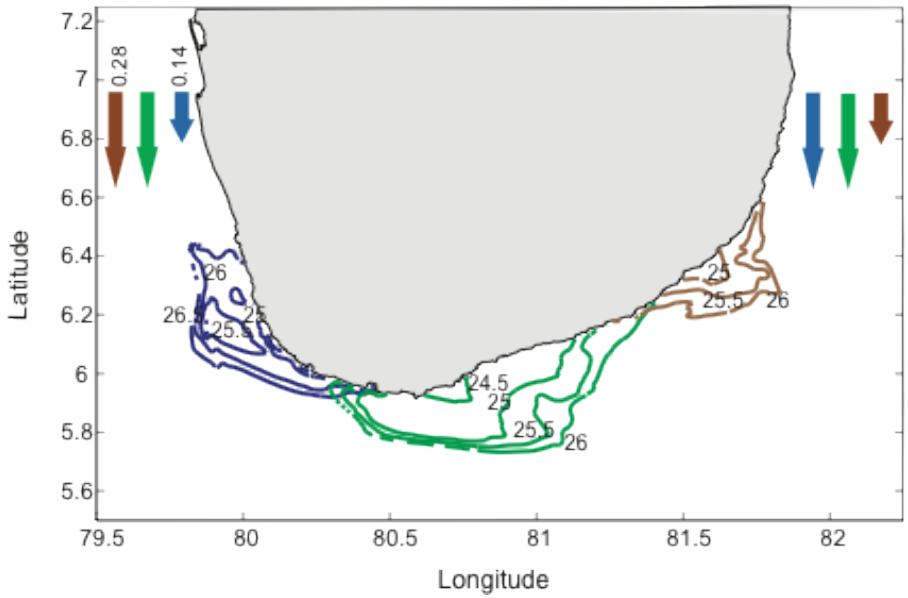

Fig. 14. Predicted locations of the convergence region and associated upwelling region with respect to different stress along each coast.

BGD
10, 14953–14998, 2013

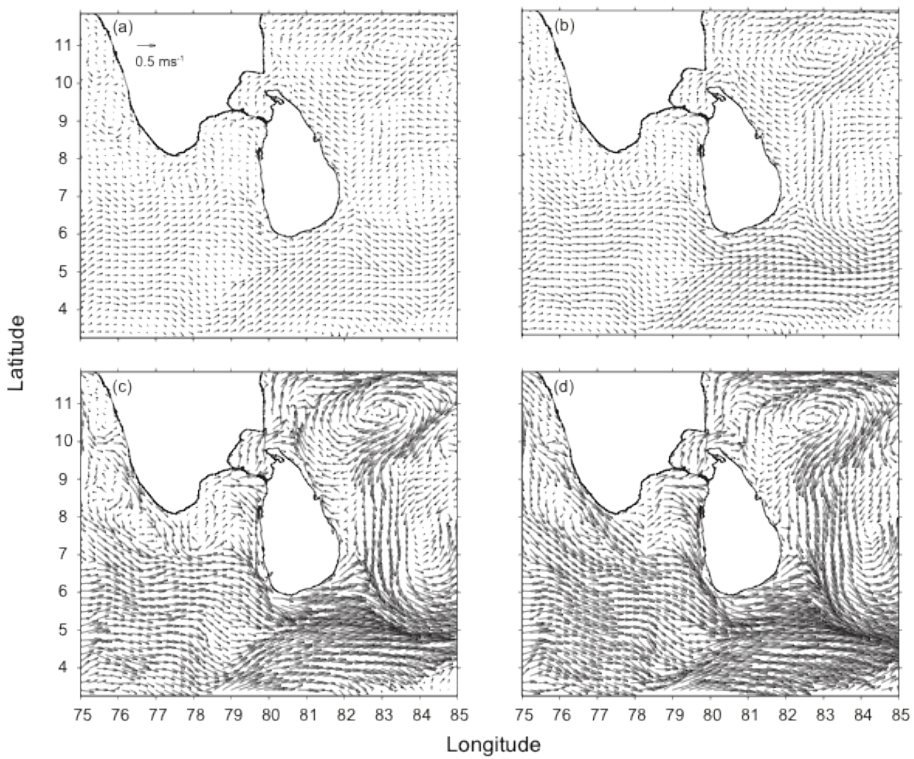

Fig. 15. Predicted surface currents under constant westerly winds at **(a)** 2 ms^{-1}; **(b)** 4 ms^{-1}; **(c)** 6 ms^{-1}; and, **(d)** 8 ms^{-1}.

BGD
10, 14953–14998, 2013

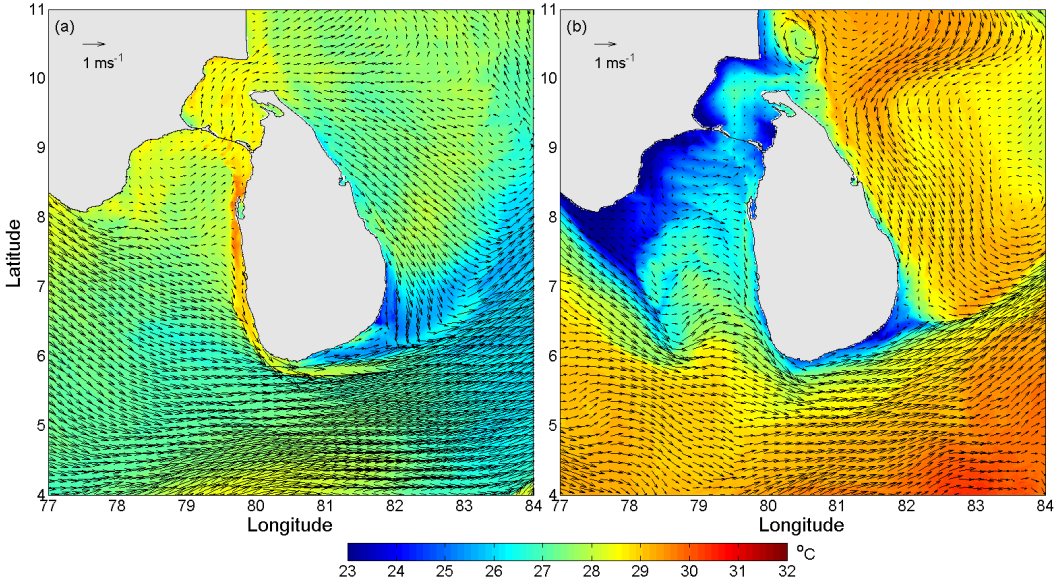

Fig. 16. Predicted near-surface current vectors plotted on the surface temperature field on 15 June 2011. **(a)** simulation including Coriolis forcing; and, **(b)** simulation excluding Coriolis forcing.

BGD
10, 14953–14998, 2013